
Article:
Shui, W., Zhou, M., Maddock, S.C. et al. (2017) A PCA-Based Method for Determining Craniofacial Relationship and Sexual Dimorphism of Facial Shapes. Computers in Biology and Medicine, 90. pp. 33-49. ISSN: 0010-4825

https://doi.org/10.1016/j.compbiomed.2017.08.023

A PCA-Based Method for Determining Craniofacial Relationship and Sexual Dimorphism of Facial Shapes

Wuyang Shui[1,2], Mingquan Zhou[1,2], Steve Maddock[3], Taiping He[4], Xingce Wang[1,2], Qingqiong Deng[1,2*]

1.College of Information Science and Technology, Beijing Normal University, Beijing, 100875, China;
2.Beijing Key Laboratory of Digital Preservation and Virtual Reality for Cultural Heritage, Beijing, China;
3.Department of computer science, Sheffield University, Sheffield, S1 4DP, United Kingdom;
4.Affiliated Hospital of Shaanxi University of Chinese Medicine, Xianyang, 712000, China;

Abstract: Previous studies have used principal component analysis (PCA) to investigate the craniofacial relationship, as well as sex determination using facial factors. However, few studies have investigated the extent to which the choice of principal components (PCs) affects the analysis of craniofacial relationship and sexual dimorphism. In this paper, we propose a PCA-based method for visual and quantitative analysis, using 140 samples of 3D heads (70 male and 70 female), produced from computed tomography (CT) images. There are two parts to the method. First, skull and facial landmarks are manually marked to guide the model's registration so that dense corresponding vertices occupy the same relative position in every sample. Statistical shape spaces of the skull and face in dense corresponding vertices are constructed using PCA. Variations in these vertices, captured in every principal component (PC), are visualized to observe shape variability. The correlations of skull- and face-based PC scores are analysed, and linear regression is used to fit the craniofacial relationship. We compute the PC coefficients of a face based on this craniofacial relationship and the PC scores of a skull, and apply the coefficients to estimate a 3D face for the skull. To evaluate the accuracy of the computed craniofacial relationship, the mean and standard deviation of every vertex between the two models are computed, where these models are reconstructed using real PC scores and coefficients. Second, each PC in facial space is analysed for sex determination, for which support vector machines (SVMs) are used. We examined the correlation between PCs and sex, and explored the extent to which the choice of PCs affects the expression of sexual dimorphism. Our results suggest that skull- and face-based PCs can be used to describe the craniofacial relationship and that the accuracy of the method can be improved by using an increased number of face-based PCs. The results show that the accuracy of the sex classification is related to the choice of PCs. The highest sex classification rate is 91.43% using our method.

Keywords: Computed tomography (CT); dense corresponding vertices; statistical shape spaces; shape variability; craniofacial relationship; sexual dimorphism

1. Introduction

Facial appearance and the geometric shape of the mouth, nose, and eyes are affected by the geometry of the bony structures [1]. Medical images provide a considerable amount of information that allows researchers to investigate the craniofacial relationship between the skull and face [2-6], face shape variability [7-11], bone shape variability [12], and brain morphology[13].

To establish the craniofacial relationship, analysis of facial soft tissue thickness (FSTT) at anatomical landmarks has been used in medical image and digital models [14, 15]. FSTT is affected by many factors, such as age, sex, body mass index (BMI), and ethnicity (see [16-20]for a summary of the statistical descriptors and regression equations of FSTT at every landmark.) The disadvantage of this method is that no standard criteria exist for choosing the anatomical landmarks [5, 21] and manual acquisition of the FSTT measurements is a tedious task [22]. Although an alternative method exists, in which the densely calculated FSTT of every vertex is taken [23, 24], describing the craniofacial relationship among all the samples remains a challenge.

To address the limitations of the above FSTT methods, regression is a prominent technique that can be used to map the statistical shape spaces of the skull and face [3-5, 25-28]. Because of the large number of vertices (>100,000), statistical shape spaces are first constructed using principal component analysis (PCA), and the PCs and corresponding PC scores are computed. Every vertex of the skull and face is projected onto low-dimension linear subspaces, and then, the skull-based and corresponding face-based PC scores are used to quantify shape variation. Several classic machine learning techniques have been used to establish the craniofacial relationship, based on the skull- and face-based PC scores, for example, support vector regression [4, 25], latent root regression [5], and partial least squares regression (PLSR) [3, 26-29]. However, few papers have described the shape variation of the skull and face or discussed the reason why linear regression is used to investigate craniofacial relationships. In addition, the extent to which the choice of PCs influences the computation of the craniofacial relationship needs to be investigated.

Previous studies have investigated the sexual dimorphism of face shape variation, where a strong relationship between facial size and sexual dimorphism was shown [30-32]. The effects on face shape variation related to age [7], population [33], and genetic association [34] have been extensively studied. Point distribution model (PDM) and geometric morphometric (GMM) techniques have been widely used to statistically and visually understand face shape variation based on a few anatomical landmarks [8, 29, 32, 35]. Visualization of the relationship between facial features, captured in every PC, has been used to analyse craniofacial morphometric changes[8]. In recent years, dense corresponding vertices have been used [30, 31] because the use of landmarks decreases statistical power and negatively affects shape change analysis [34]. To predict the sex of an individual from a given facial shape, several classification methods have been used for digital models, such as step-wise discrimination, linear discriminant analysis, and adaptive boosting (Adaboost) [35-37]. However, when using laser scanning and neuroimaging, shape differences do exist between facial models because of gravity[38], and new findings from the neuroimaging data of such facial models should be considered.

In this paper, we propose a visual and quantitative method to analyse the craniofacial relationship and investigate the face shape variability of sexual dimorphism using dense corresponding vertices. Visualization of skull and face shape variability, captured in every PC, is conducted to determine the extent to which PCs quantify the craniofacial relationship. We analyse the correlation between skull- and face-based PC scores, and linear regression is used to represent the craniofacial relationship. We compare the mean and standard deviation of every vertex and explore the effect of the choice of PCs on the accuracy of craniofacial relationship computation. In addition, we analyse the manner in which every PC affects face shape variability. We predict the sex of a given face using support vector machines (SVMs), and analyse the extent to which the choice of PCs affects sex classification.

Section 2 will describe the materials and methods used in our work. Section 3 will present the results and Section 4 will critically discuss these. Finally, Section 5 will give the conclusions.

2. Materials and Methods

2.1 Materials

A total of 140 living individuals (70 male and 70 female) of Han Chinese nationality having normal craniofacial morphology were recruited for the study [3, 24]. All the study participants were aged between 20 and 60 years; many were residents of the Xi'an, Shaanxi province. Medical images were acquired using the clinical multi-slice computed tomography (CT) scanner system (Siemens Sensation 16) belonging to the Affiliated Hospital of Shaanxi University of Chinese Medicine. Standard DICOM 3.0 images, with a resolution of 512 × 512, were used for all samples. The Institutional Review Board (IRB) of the Affiliated Hospital of Shaanxi University of Chinese Medicine approved the study. All participants were provided with full details of the study and gave written informed consent.

To eliminate the influence of the brain and interior structure of the skull, the exterior boundary was extracted from CT images, and exterior triangular meshes of both skull and face were generated [39]. To remove the inconsistency in position and pose, every sample was transformed into a standardized Frankfurt Horizontal coordinate system, consisting of four skull landmarks: the left porion (*Lp*), right porion (*Rp*), left orbital (*Lo*), and glabella (*G*). A total of 78 anatomical landmarks and corresponding facial landmarks were defined and marked on the skull and face [24]. Fig. 1 shows the skull and corresponding face models in the Frankfurt coordinate system and Fig. 2 shows the 78 skull landmarks and their corresponding facial landmarks. The registration of the skull and face directly affects the quality of the dense corresponding vertices and the construction of statistical shape spaces. Taking these landmarks as a guide, the iterative closest point (ICP) with scaling, generic thin-plate spline (TPS), and compact support radial basis function (CSRBF) methods were applied to register a reference skull (or face) and a target skull (or face). The registration process is described in our previous paper [24].

2.2 Methods

This paper presents a visual and quantitative PCA-based method for determining the craniofacial relationship and the sexual dimorphism of face shape variation (Fig. 3). The procedures are as follows: (a) the statistical shape spaces of the skull and face are constructed from dense corresponding vertices, transforming shapes from Cartesian coordinates to low-dimension shape parameter spaces; (b) variations in the dense corresponding vertices of the skull and face, captured in every PC, are visualized; (c) the correlation of skull- and face-based PC scores are analysed by partial least squares (PLS) analysis; (d) the linear regression method is applied to fit the craniofacial relationship based on the PC scores of skulls and corresponding faces. We compute the PC coefficients of a face based on a combination of this craniofacial relationship and the PC scores of a skull, and apply these coefficients to estimate a 3D face. To evaluate the accuracy of the method, the mean and standard deviation of every vertex between two models were calculated, where the two models were reconstructed by using PC scores and PC coefficients, respectively; (e) each PC in the facial space is analysed for sex determination using SVMs. We examined the effects of the PCs as related to sexual dimorphism.

2.2.1 Statistical Shape Space

A number of basis functions can be generated as a shape space that fits a probability distribution to shape space coefficients, and the results can be used to analyse 3D data [40]. PCA was considered the most appropriate method to construct statistical shape spaces of the skull (or face), after the dense corresponding vertices of the skull (or face) for every sample within our dataset had been established. PCA was applied to simplify each sample in our dataset by using average skull (or face) vertex coordinates, linear combinations of PC scores and corresponding orthogonal PCs. The skull and face vertices of each sample are denoted by $\mathrm{S}=\{[x_{i,1}^{\mathrm{S}}, y_{i,1}^{\mathrm{S}}, z_{i,1}^{\mathrm{S}},...,x_{i,m}^{\mathrm{S}}, y_{i,m}^{\mathrm{S}}, z_{i,m}^{\mathrm{S}}]^{\mathrm{T}}, i=1,2,3,...,\mathrm{N};\}$ and $\mathrm{F}=\{[x_{i,1}^{\mathrm{F}}, y_{i,1}^{\mathrm{F}}, z_{i,1}^{\mathrm{F}},...,x_{i,\mathrm{n}}^{\mathrm{F}}, y_{i,\mathrm{n}}^{\mathrm{F}}, z_{i,\mathrm{n}}^{\mathrm{F}}]^{\mathrm{T}}, i=1,2,3,...,\mathrm{N};\}$, where *N*, *m*, and *n* denote the number of samples within the dataset, the number of skull vertices, and the number of face vertices, respectively.

The skull vertex coordinates of each sample are represented by

$$S(\mathbf{a}) = \overline{S} + \sum_{i=1}^{\mathrm{N}-1} \mathbf{a}_i \mathbf{v}_i \tag{1}$$

where $\overline{S}$ denotes the average skull, $\mathbf{a}=[\mathbf{a}_1,\mathbf{a}_2,\mathbf{a}_3,...,\mathbf{a}_{\mathrm{N}-1}]$ denotes the PC scores, consisting of the eigenvalues in descending order, and $\mathbf{v}=[\mathbf{v}_1,\mathbf{v}_2,\mathbf{v}_3,...,\mathbf{v}_{\mathrm{N}-1}]\in\mathbb{R}^{3\mathrm{m}\times(\mathrm{N}-1)}$ denotes the corresponding orthogonal PCs.

The corresponding face vertex coordinates of each sample are represented by

$$F(\mathbf{b}) = \overline{F} + \sum_{i=1}^{\mathrm{N}-1} \mathbf{b}_i \mathbf{w}_i \tag{2}$$

where $\overline{F}$ denotes the average face, $\mathbf{b}=[\mathbf{b}_1,\mathbf{b}_2,\mathbf{b}_3,...\mathbf{b}_{N-1}]$ denotes the PC scores, consisting of the eigenvalues in descending order, and $\mathbf{w}=[\mathbf{w}_1,\mathbf{w}_2,\mathbf{w}_3,...,\mathbf{w}_{N-1}]\in\mathbb{R}^{3n\times(\mathrm{N}-1)}$ denotes the corresponding orthogonal PCs.

To investigate the effect of each PC on the skull (or face) variation, the coordinates of each vertex on the newly generated face were defined as

$$F(\lambda) = \overline{F} + 3\lambda\sigma_i \mathbf{w}_i \tag{3}$$

where σ_i denotes the standard deviation of the *i*th PC, and the weighting coefficient of PC λ is set to -1.0, -0.6, -0.2, 0.2, 0.6, and 1.0.

The use of dense corresponding vertices means that the dimension of each vector is excessively large (>300,000), and therefore, we used Turk's method to solve the covariance matrix [39]. After the PC scores and corresponding PCs of the skull (or face) were obtained, the geometrical coordinates of every skull (or face), denoted by *PCAskull* (or *PCAface*), were calculated. To evaluate the accuracy of the PCA representation, the quantitative error of each vertex between the real skull (or face) and the *PCAskull* (or *PCAface*) was calculated by

$$error_j = \frac{1}{N}\sum_{i=1}^{N}\sum_{j=1}^{k}\left\| p_{i,j} - p_{i,j}^{pca} \right\| \tag{4}$$

where $p_{i,j}=(x_{i,j},y_{i,j},z_{i,j})$ and $p_{i,j}^{pca}=(x_{i,j}^{pca},y_{i,j}^{pca},z_{i,j}^{pca})$ denote the *j*th vertex of the *i*th sample, respectively, the *i*th skull (face) is represented by PC scores, and *k* denotes the number of vertices.

This procedure was repeated for all the samples in the dataset, and the average (*avergError*) of

all the error values was calculated by

$$avergError = \frac{1}{N \cdot k} \sum_{i=1}^{N} \sum_{j=1}^{k} \left\| p_{i,j} - p_{i,j}^{pca} \right\| \tag{5}$$

where N and k denote the number of samples and the number of vertices of every sample, respectively.

In addition, the standard deviation of each vertex of all the samples between the real skull (or face) and the skull (or face) computed by PC scores was calculated. And the average (*avergStd*) of all the standard deviation values of all the samples was calculated.

2.2.2 Computation of Craniofacial Relationship

PLS provides a method to visualize related variations after decomposition of shape components in different axes. PLS analysis has previously been applied to 3D facial morphology and facial organs (such as mouth, nose and eyes) [7, 29, 33]. In comparison to PCA, PLS maximizes the covariance and thus identifies the components that are more relevant. Skull- and face-based PC scores are represented by $\mathbf{Skull}_{l \times p} = [\boldsymbol{\alpha}_{1,p}, \boldsymbol{\alpha}_{2,p}, ..., \boldsymbol{\alpha}_{l,p}]$ and $\mathbf{Face}_{l \times q} = [\mathbf{b}_{1,q}, \mathbf{b}_{2,q}, ..., \mathbf{b}_{l,q}]$, where l denotes the number of samples within the database, p denotes the number of selected skull-based PCs, and q denotes the number of selected face-based PCs. PLS was applied to skull- and face-based PC scores to find the correlation.

The craniofacial relationship of the samples in our dataset were quantitatively computed by optimizing the following equation

$$\mathbf{M} = \arg\min \left\| \mathbf{Skull} \times \mathbf{M} - \mathbf{Face} \right\|^2 + \delta^2 \left\| \mathbf{M} \right\|^2 \tag{6}$$

where $\mathbf{M}$ denotes the $p \times q$ matrix of regression coefficients and the weighting coefficient is δ.

When the PC scores of a skull in our dataset were provided, the PC coefficients of the corresponding face were calculated based on the craniofacial relationship. The coordinates of the estimated face (*estimatedface*) were then calculated, where the PC coefficients were multiplied by the corresponding face-based PCs and added to the coordinates of the average face model.

To quantitatively evaluate the accuracy of the computed craniofacial relationship, we calculated the quantitative error of each vertex between the *PCAface* and *estimatedface*. This procedure was repeated for each sample, and the average (*avergEstimate*) was defined by calculating the quantitative errors of all the samples. In addition, the standard deviation of each vertex was calculated and the average (*avergEstimateStd*) was defined by calculating the standard deviation values of all the samples. To analyse the interplay between the choice of PCs and the accuracy of the computed craniofacial relationship, we fitted a map **M** by fixing the skull-based PCs and increasing the number of face-based PCs. Subsequently, we created the *estimatedface* using this fitted map **M** and compared *avergEstimate* and *avergEstimateStd*.

2.2.3 Face Shape Variability of Sexual Dimorphism

Although several studies based on PCA confirmed that the sex of a person has a significant influence on face shape, sex determination according to PCs was not clearly shown [30, 31]. In our method, the PC scores of every sample within our dataset were calculated and the sex label of every sample was set to 1 (male) or -1 (female). To determine the PCs that best illustrate the distinction

between male and female samples, one-way analysis of variance (ANOVA) was first applied to each PC to observe any significant difference.

We applied SVMs to the face-based PC scores of dense corresponding vertices (DCS-SVMs) to solve the problem of two-class pattern classification, and predicted the sex of a given face. The basic principle of SVMs is that they search a linear separating hyperplane, with the maximal margin, by mapping the input data into a higher dimensional space. The radial basis function (RBF) kernel nonlinearly maps samples into a higher dimensional space to overcome the problem that the relationship between class labels and attributes is nonlinear, and face-based PC scores are approximated by Gaussian distribution, similar to the RBF kernel [41, 42]. Therefore, SVMs with an RBF kernel $k(x_i, x_j) = \exp(-|x_i - x_j| / 2\delta^2)$ were used as the classifier, where δ is the width of the Gaussian cluster. In our method, we use LIBSVM to create SVMs and optimize all the parameters [43].

To investigate whether the choice of PCs affects the accuracy of sex determination, the sex classifier was repeatedly executed, with an increased number of face-based PCs. To evaluate the generalizability of the model fitting, we applied 5-fold cross-validation to the dataset for the sex determination. All the faces were randomly divided into five groups, where each group consisted of 50% males and 50% females. A classifier was then constructed, based on four groups using SVMs, and each face of the remaining group was used as a test sample.

In this study, dense corresponding vertices were constructed on the skulls and faces in our dataset. Visualization of the shape variability, captured in every PC, was done using C++ and OpenGL, and the computation of the craniofacial relationship and the sex determination were done using MATLAB R2012b.

3. Results

3.1 Statistical Shape Spaces

Each skull (or face) has been represented by PCA and the PCs are sorted according to the descending order of eigenvalues. To represent a skull (or face), we use the terminology PCs i, where i is the first i PCs in the list. For statistical shape spaces of the skull, a total of 49 (PCs 49), 50 (PCs 50), and 83 (PCs 83) PCs accounted for over 98% of variance in the male dataset, female dataset and the dataset containing both sexes, respectively. For the statistical shape spaces of the face, a total of 35 (PCs 35), 39 (PCs 39), and 52 (PCs 52) PCs accounted for over 98% variance in the male dataset, female dataset and the dataset containing both sexes, respectively. To show the representation accuracy achieved by using PCA, **t**he average and standard deviation of every vertex of all the samples within our dataset are depicted in graphical format with a colour bar using PCs 1, PCs 10, PCs 20, PCs 30, and PCs 35 (Figs. 4 and 5). Figs. 6a and 6b show *avergError* and *avergStd* values, respectively, when the number of face-based PCs was increased. These results show that *avergError* value decreases with an increased number of PCs, because more shape detail is contained when a larger number of PCs are employed.

3.2 Shape Variation in the Skull and Face

To examine the potential shape differences that constitute sexual dimorphism, the visualizations of the skull (or face), captured in each single PC were created (see Figs. 7 and 8). These are denoted as PC$i\pm$, where i indicates the i index of the PC, PCi+ denotes the weighting coefficient λ as 1.0, and

PC*i*- denotes the weighting coefficient λ as -1.0.

Fig. 7 shows the skull shape variation related to PC1, PC2, PC3, PC4, and PC5. The two leading PCs reflect 46.59% of the total variability. A comparison of PC1+ and PC1- reveals that a decrease in PC1's score is related to an enlargement and widening of the skull. A comparison of PC2+ and PC2- reveals that a decrease in PC2's score is connected to lengthening and narrowing in the lower third of the skull, as well as to the convexity of the skull forehead. A decrease in PC3's score seems to explain the widening of the upper third of the skull, and mandible contraction. A decrease in PC4's score seems to be related to a narrower and shorter upper third of the skull, but indicates that the back of the skull is convex. A decrease in PC5's score appears to explain a narrower upper third and shorter bottom third of the skull.

Fig. 8 shows the face shape variation related to PC1, PC2, PC3, PC4, and PC5, with the two leading PCs reflecting 49.64% of the total variability. A comparison of PC1+ and PC1- reveals that a decrease in PC1's score is related to a narrower and shorter face, as well as to a narrower neck, whereas a decrease in PC2's score is related to a lengthening and wider face. A comparison of PC3+ and PC3- reveals that a decrease in PC3's score is connected to lengthening and narrowing of the lower third of the face, as well as to forehead convexity. A comparison of PC4+ and PC4- reveals that a decrease in PC4's score is connected to a shorter and wider lower third of the face. A decrease in PC5's score appears to represent a widening upper third and narrower bottom third of the face.

Overall, the comparison between skull- and face-based PCs reveals that skull-based PC1 and face-based PC2 and skull-based PC2 and face-based PC3 appear to explain shape variation along a similar direction (Fig. 9).

3.3 Computation of Craniofacial Relationship

PC scores were used to quantify the shape variation in both the skull and face, and PLS was used to quantitatively examine the correlations between skull- and face-based PC scores for every sample in the dataset (Fig. 10a). An example of the first PLS axes is depicted in Fig. 10b; it indicates that there exists an approximate linear relationship between t1 and u1, and thus, a multivariate linear regression can be used to determine the craniofacial relationship between skull- and face-based PC scores.

Since the sex of the subject plays a significant role in the craniofacial relationship, we separated the database into two groups: skull-based PCs 49 and face-based PCs 35 for males and skull-based PCs 50 and face-based PCs 39 for females. Fig. 11 shows examples of the *estimatedface* models when the number of face-based PCs is increased. Fig. 12 shows the quantitative error and standard deviation of every vertex between *PCAface* and *estimatedface*, using face-based PCs 1, PCs 10, PCs 20, PCs 30, and PCs 35, which were used to assess the number of PCs that affect the accuracy of the craniofacial relationship. Fig. 13 shows the *avergEstimate* and *avergEstimateStd* values, with an increased number of face-based PCs. These results indicate that the *avergEstimate* and *avergEstimateStd* values of both sexes decrease when the number of face-based PCs is increased.

The purpose of craniofacial reconstruction is to generate a life-like 3D facial appearance for an unidentified skull. To validate the effectiveness of our computed craniofacial relationship application in craniofacial reconstruction, the leave-one-out cross validation was used, i.e., each sample in our database was chosen as a test case, and the other samples were used as training dataset for map fitting. Fig. 14 shows some of the best examples of the estimated facial appearances using face-based PCs 35 for males and face-based PCs 39 for females. Fig. 15 shows the geometric deviations of every vertex

between *PCAface* and *estimatedface*. The *avergEstimate* was 4.88 mm for females and 5.56 mm for males.

3.4 Face Shape Variation Related to Sex

As seen in Fig. 8, it seems that sexual dimorphism is differentiated in the negative and the positive directions in the first two PCs. To quantitatively test the significant difference between the sex and every PC, ANOVA was applied to the samples of both sexes. The sex classification and significant differences in each PC are illustrated in Fig. 16a. SVMs were conducted to illustrate their influence on sexual dimorphism (Fig. 16b). The results for PC1, PC2, and PC18 are all statistically significant ($p < 0.005$), and correspond to the highest correct sexual classification. Fig. 17 shows the face shape variation related to PC18 and depicts the sex dimorphism between the negative and positive directions. To ascertain the effect of the choice of PCs on the accuracy of the sex classification, 5-fold cross-validation was performed, with DCS-SVMs and linear discriminant analysis being applied to dense corresponding vertices (DCS-linear), as shown in Fig. 18. The highest sex classification accuracy of DCS-SVMs was almost 91.43%, corresponding to PCs 19, and the highest sex classification accuracy of DCS-linear was 90.71%, corresponding to PCs 33. We also applied SVMs to the landmarks (Landmarks-SMVs), which yielded the highest correct sex classification accuracy is 86. 83%.

4 Discussion

The craniofacial relationship and the sexual dimorphism of face shape variation play a significant role in the fields of forensic science and anthropology. In this study, PCA was used to construct the statistical shape spaces of the skulls and faces in our dataset, and the visual and quantitative PCA-based method was used to analyse the effectiveness of PC scores in quantifying the skull and face shape variability. We described the use of PC scores to represent the craniofacial relationship by a linear regression for all the samples in our dataset, and showed the influence of the use of PCs on face shape variability and the expression of sexual dimorphism.

Because manually marked landmarks are more accurate in terms of their positioning, PDM [44] and GMM [29] derived from a limited number of landmarks have been widely used for face shape variation analysis. To capture more detail, the use of dense corresponding vertices of the skull and face is a potential solution. Owing to the complex shapes involved, it remains a challenge to establish homologous, dense one-to-one corresponding vertices of the skull and face. Model alignment techniques have been used to obtain a close match between templates and other models, where the closest point is always taken as the corresponding vertex. The widely used rigid and non-rigid registration methods have been applied to improve the accuracy of registration, for example, generalized Procrustes analysis (GPA) and TPS [22, 30, 31], ICP and TPS [45, 46], TPS and CSRBF [3], TPS–RPM [47], and statistical model-based registration [2, 26]. In our study, facial and skull landmarks were manually marked to improve the registration accuracy and obtain high quality corresponding vertices between different samples. However, because landmarks are lacking at the back of the head and the shape around the neck varies, low quality corresponding vertices always occurred in these regions.

PCs were used to visualize and analyse face shape variation in previous studies [8, 9, 31, 33, 48]. The correlation between face shape variation and properties related to sex, age, population, etc. has been investigated, with the facial geometrical shapes related to each single PC being visualized.

However, few studies have visually investigated the craniofacial relationship in terms of PCs. In our study, to investigate the correlation between the skull and face, both skull and face shape variation, corresponding to each single PC, were first visualized. The shape variation from PC1 to PC5 showed that the pairs skull-based PC1 and face-based PC2 and skull-based PC2 and face-based PC3 seem to have a related shape influence. Although face-based PC1 explains the widening and enlargement of the face, it also explains the variation in the neck shape. In a previous study [29], the correlation between bony and cutaneous landmark configurations was analysed using the two-blocks PLS method. We extended the PLS analysis to quantitatively detect correlations between the skull- and face-based PC scores. We found an approximate linear relationship between the skull- and face-based PC scores, and therefore, the multivariate linear regression was used to determine the craniofacial relationship.

PC scores have been used to quantify skull and face shape variation, and therefore, the craniofacial relationship has been computed by learning a mapping between skull- and corresponding face-based PC scores [3-5, 25-29]. However, few studies have investigated the influence of the choice of PCs on the obtained accuracy of the craniofacial relationship. Understanding and quantifying the impact of the PCs will help to improve the accuracy of PCA-based craniofacial relationship computation. In our study, the skull-based PC scores of each sample in our dataset were taken as the independent variable, and the corresponding face-based PC scores were taken as the dependent variable. Linear regression was used to compute the mapping between skull- and face-based PC scores and the number of face-based PCs was varied. In previous studies, the accuracy of the mapping was assessed using the geometrical error between the *estimatedface* and the closest points on the real face. To improve on this, we compared the quantitative error and standard deviation of every vertex, *avergEstimate* and *avergEstimateStd* between *estimatedface* and *PCAface*. The geometric deviations of the majority of regions are smaller when all the samples were used as training dataset, and the regions for which the results were most inaccurate were those around the ears and neck. This demonstrates that linear regression is suitable for fitting the craniofacial relationship. In addition, both *avergEstimate* and *avergEstimateStd* of geometric deviations decreased when the number of PCs was increased, because more geometrical details were used for map fitting.

We used the leave-one-out cross validation to assess the predictability of the fitted mapping. As seen in Fig. 15, larger geometric deviations were observed around the cheek, which illustrates that the fitted craniofacial relationship derived from the training dataset is not complete consistent with test skull in this region. This finding was demonstrated in the studies presented in [18, 24], which showed that the largest and most notable variation is observed around the cheek, and FSTT is affected by the sample properties (such as sex, age, BMI, etc.). These properties should be considered to improve the prediction ability of the map fitting. In addition, larger geometric deviations are still observed around the top of the head, because the skull shape variation is not completely consistent with the face shape variation in this region, despite the FSTT being smaller. The highest geometric deviations were observed around the ears and neck. One probable explanation for this is that the geometrical shapes of the neck and ears weakly correlate with the corresponding bones. Since our previous work has presented that the most obvious reconstruction errors happened in the front of head, which need to pay more attention[3, 24], the reconstruction errors in this region have been further analysed. Almost 56% of the front vertices showed deviations that were less than 5.0 mm for females, and 42% showed deviations that were less than 5.0 mm for males. In

comparison to the case where all the samples were used as a training dataset, the geometric deviations were much larger using leave-one-out cross validation.

Studies in the literature [8, 30-32] confirm the sexual dimorphism of facial shape, i.e. that the average size of the male face is greater than the female face. Chakravarty et al. evaluated the effect of the sex and age of a person on the PCs of face landmarks, and demonstrated that each PC encodes a different relationship between facial features [8]. Logistic regression was performed to determine which combination of PCs of facial landmarks distinguished males and females [32]. Mydlová et al. used a two-way MANOVA to analyse the dependence of facial shape on sex and age, and showed that both factors significantly influence the facial form and shape [31]. Velemínská et al. revealed that facial variability was characterized by a strong relationship between the facial size and the shape of sexual dimorphic traits, and they used discriminant function analysis to assess the sex classification accuracy for PC1 and PC2 [30]. In our paper, we have proposed a visual and quantitative analysis applied for each PC. Tests were conducted to examine whether significant differences related to sex exist; SVMs were used to compute the sex classification. The visualization of PC$i\pm$ was used to show significant differences in the analysis and sex classification results. The results showed a significant difference between the PC scores and sex ($p < 0.005$) and the highest sex classification accuracy of PC1 and PC2 confirmed that face size is strongly correlated with sex. In addition, we observed that PC18 ($p < 0.005$) was strongly correlated with the sex of a person, corresponding to lengthening in the lower third of the face, and broadening of the mouth and chin, and these attributes make the face appear more masculine.

PC scores have been widely used for sex classification in previous studies [35, 49, 50]. In our study, to evaluate the PCs' impact on sex determination, training and testing steps were performed using a 5-fold cross-validation experiment. The results showed that sex can be identified based on PC scores, and the accuracy for determining sexual dimorphism was related to the choice of PCs. For 2D appearance-based sex classification, the performance of SVMs has been demonstrated to be superior to other traditional pattern classifiers, for example, linear, Fisher linear discriminant, and radial basis function (RBF) classifiers [51]. Therefore, we extended SVMs to construct sex classifiers for 3D faces. According to the results of our experiments, sex classification accuracy is related to the choice of PCs, and the highest sex classification accuracy was 91.43%, corresponding to PCs 19. The use of SVMs with an RBF kernel was more effective than that of linear discriminant analysis, and the use of dense corresponding vertices was more effective than that of landmarks.

5 Conclusion

In our study, we have applied PCA to dense correspondence vertices to reduce data dimensions and have proposed a visual and quantitative PCA-based method to analyse the craniofacial relationship and facial sexual dimorphism. We analysed the correlation between skull- and face-based PC scores so that linear regression could be used to represent the craniofacial relationship. The accuracy of the craniofacial relationship computation increased when a larger number of face-based PCs were used. We examined the correlation between PCs and sex classification, and explored the impact of the choice of PCs on the expression of sexual dimorphism. Sex classification accuracy is related to the choice of PCs, and the highest sex classification accuracy achieved was 91.43%. Although linear regression successfully fitted the mapping between the skull- and face-based PC scores of all the samples in our dataset, it remains a challenge to improve the prediction ability. Further studies should be conducted to address the problem of over-fitting, and

improve the accuracy of craniofacial reconstruction.

Conflict of interest

None declared.

Acknowledgement

The authors would like to thank the anonymous reviewers. This work was supported by the National Nature Science Foundation of China (No.61402042), Beijing Natural Science Foundation (No.4152028), and Chinese Academy of Sciences (CAS) Interdisciplinary Innovation Team.

References

[1] C. Wilkinson, Computerized forensic facial reconstruction, Forensic science, medicine, and pathology, 1 (2005) 173-177.

[2] F. Duan, Y. Yang, Y. Li, Y. Tian, K. Lu, Z. Wu, M. Zhou, Skull identification via correlation measure between skull and face shape, IEEE Transactions on Information Forensics and Security, 9 (2014) 1322-1332.

[3] Q. Deng, M. Zhou, Z. Wu, W. Shui, Y. Ji, X. Wang, C.Y.J. Liu, Y. Huang, H. Jiang, A regional method for craniofacial reconstruction based on coordinate adjustments and a new fusion strategy, Forensic science international, 259 (2016) 19-31.

[4] P. Paysan, M. Lüthi, T. Albrecht, A. Lerch, B. Amberg, F. Santini, T. Vetter, Face Reconstruction from Skull Shapes and Physical Attributes, Lecture Notes in Computer Science, Pattern Recognition, Springer, Berlin/Heidelberg (2009) 232-241.

[5] M. Berar, F.M. Tilotta, J.A. Glaunès, Y. Rozenholc, Craniofacial reconstruction as a prediction problem using a Latent Root Regression model, Forensic science international, 210 (2011) 228-236.

[6] P. Claes, D. Vandermeulen, S. De Greef, G. Willems, J.G. Clement, P. Suetens, Computerized craniofacial reconstruction: Conceptual framework and review, Forensic science international, 201 (2010) 138-145.

[7] W. Chen, W. Qian, G. Wu, W. Chen, B. Xian, X. Chen, Y. Cao, C.D. Green, F. Zhao, K. Tang, Three-dimensional human facial morphologies as robust aging markers, Cell research, 25 (2015) 574-587.

[8] M.M. Chakravarty, R. Aleong, G. Leonard, M. Perron, G.B. Pike, L. Richer, S. Veillette, Z. Pausova, T. Paus, Automated analysis of craniofacial morphology using magnetic resonance images, PloS one, 6 (2011) e20241.

[9] K. Marečková, Z. Weinbrand, M.M. Chakravarty, C. Lawrence, R. Aleong, G. Leonard, M. Perron, G.B. Pike, L. Richer, S. Veillette, Testosterone-mediated sex differences in the face shape during adolescence: subjective impressions and objective features, Hormones and behavior, 60 (2011) 681-690.

[10] K. Marečková, M.M. Chakravarty, M. Huang, C. Lawrence, G. Leonard, M. Perron, B.G. Pike, L. Richer, S. Veillette, Z. Pausova, Does skull shape mediate the relationship between objective features and subjective impressions about the face?, NeuroImage, 79 (2013) 234-240.

[11] E.F. Kranioti, M.Y. İşcan, M. Michalodimitrakis, Craniometric analysis of the modern Cretan population, Forensic science international, 180 (2008) 110. e111-110. e115.

[12] E. Nicholson, K. Harvati, Quantitative analysis of human mandibular shape using three-dimensional geometric morphometrics, American journal of physical anthropology, 131 (2006) 368-383.

[13] X. Wu, W. Liu, W. Dong, J. Que, Y. Wang, The brain morphology of Homo Liujiang cranium fossil by three-dimensional computed tomography, Chinese Science Bulletin, 53 (2008) 2513-2519.

[14] Y. Dong, L. Huang, Z. Feng, S. Bai, G. Wu, Y. Zhao, Influence of sex and body mass index on facial soft tissue thickness measurements of the northern Chinese adult population, Forensic science international, 222 (2012) 396.e391-397.

[15] D. Cavanagh, M. Steyn, Facial reconstruction: soft tissue thickness values for South African black females, Forensic science international, 206 (2011) 215.e211-217.

[16] C.N. Stephan, E.K. Simpson, Facial soft tissue depths in craniofacial identification (part I): An analytical review of the published adult data, Journal of forensic sciences, 53 (2008) 1257-1272.

[17] C.N. Stephan, The application of the central limit theorem and the law of large numbers to facial soft tissue depths: T-Table robustness and trends since 2008, Journal of forensic sciences, 59 (2014) 454-462.

[18] S. De Greef, P. Claes, D. Vandermeulen, W. Mollemans, P. Suetens, G. Willems, Large-scale in-vivo Caucasian facial soft tissue thickness database for craniofacial reconstruction, Forensic science international, 159 Suppl 1 (2006) S126-146.

[19] W. Jeelani, M. Fida, A. Shaikh, Facial soft tissue thickness among three skeletal classes in adult Pakistani subjects, Journal of forensic sciences, 60 (2015) 1420-1425.

[20] P. Guyomarc'h, F. Santos, B. Dutailly, H. Coqueugniot, Facial soft tissue depths in French adults: variability, specificity and estimation, Forensic science international, 231 (2013) 411.e411- e410.

[21] P. Claes, M. Walters, M.D. Shriver, D. Puts, G. Gibson, J. Clement, G. Baynam, G. Verbeke, D. Vandermeulen, P. Suetens, Sexual dimorphism in multiple aspects of 3D facial symmetry and asymmetry defined by spatially dense geometric morphometrics, Journal of anatomy, 221 (2012) 97-114.

[22] J. Guo, X. Mei, K. Tang, Automatic landmark annotation and dense correspondence registration for 3D human facial images, BMC Bioinformatics, 14 (2013) 1-12.

[23] F. Prieels, S. Hirsch, P. Hering, Holographic topometry for a dense visualization of soft tissue for facial reconstruction, Forensic science, medicine, and pathology, 5 (2009) 11-16.

[24] W. Shui, M. Zhou, Q. Deng, Z. Wu, Y. Ji, K. Li, T. He, H. Jiang, Densely Calculated Facial Soft Tissue Thickness for Craniofacial Reconstruction in Chinese Adults, Forensic science international, 266(2016) 573.e1-573.e12.

[25] Y. Li, L. Chang, X. Qiao, R. Liu, F. Duan, Craniofacial reconstruction based on least square support vector regression, IEEE International Conference on Systems, Man and Cybernetics (SMC), (2014) 1147-1151.

[26] F. Duan, D. Huang, Y. Tian, K. Lu, Z. Wu, M. Zhou, 3D face reconstruction from skull by regression modeling in shape parameter spaces, Neurocomputing, 151 (2015) 674-682.

[27] S. Shrimpton, K. Daniels, S. De Greef, F. Tilotta, G. Willems, D. Vandermeulen, P. Suetens, P. Claes, A spatially-dense regression study of facial form and tissue depth: towards an interactive tool for craniofacial reconstruction, Forensic science international, 234 (2014) 103-110.

[28] F. Duan, S. Yang, D. Huang, Y. Hu, Z. Wu, M. Zhou, Craniofacial reconstruction based on multi-linear subspace analysis, Multimedia Tools and Applications, 73 (2014) 809-823.

[29] P. Guyomarc'h, B. Dutailly, J. Charton, F. Santos, P. Desbarats, H. Coqueugniot, Anthropological Facial Approximation in Three Dimensions (AFA3D): Computer-Assisted Estimation of the Facial Morphology Using Geometric Morphometrics, Journal of forensic sciences, 59 (2014) 1502-1516.

[30] J. Velemínská, L. Bigoni, V. Krajíček, J. Borský, D. Šmahelová, V. Cagáňová, M. Peterka, Surface facial modelling and allometry in relation to sexual dimorphism, HOMO-Journal of Comparative Human Biology, 63 (2012) 81-93.

[31] M. Mydlová, J. Dupej, J. Koudelová, J. Velemínská, Sexual dimorphism of facial appearance in ageing human adults: A cross-sectional study, Forensic science international, 257 (2015) 519. e511- e519.

[32] R.J. Hennessy, A. Kinsella, J.L. Waddington, 3D laser surface scanning and geometric morphometric analysis of craniofacial shape as an index of cerebro-craniofacial morphogenesis: initial application to sexual dimorphism, Biological psychiatry, 51 (2002) 507-514.

[33] J. Guo, J. Tan, Y. Yang, H. Zhou, S. Hu, A. Hashan, N. Bahaxar, S. Xu, T.D. Weaver, L. Jin, Variation and signatures of selection on the human face, Journal of human evolution, 75 (2014) 143-152.

[34] S. Peng, J. Tan, S. Hu, H. Zhou, J. Guo, L. Jin, K. Tang, Detecting genetic association of common human facial morphological variation using high density 3D image registration, PLoS Comput Biol, 9 (2013) e1003375.

[35] A. Samal, V. Subramani, D. Marx, Analysis of sexual dimorphism in human face, Journal of Visual Communication and Image Representation, 18 (2007) 453-463.

[36] S.Z. Gilani, K. Rooney, F. Shafait, M. Walters, A. Mian, Geometric facial gender scoring: objectivity of perception, PloS one, 9 (2014) e99483.

[37] L. Ballihi, B. Ben Amor, M. Daoudi, A. Srivastava, D. Aboutajdine, Boosting 3-D-geometric features for efficient face recognition and gender classification, IEEE Transactions on Information Forensics and Security, 7 (2012) 1766-1779.

[38] A. Kustar, L. Forro, I. Kalina, F. Fazekas, S. Honti, S. Makra, M. Friess, FACE-R--a 3D database of 400 living individuals' full head CT- and face scans and preliminary GMM analysis for craniofacial reconstruction, Journal of forensic sciences, 58 (2013) 1420-1428.

[39] Q. Deng, M. Zhou, W. Shui, Z. Wu, Y. Ji, R. Bai, A novel skull registration based on global and local deformations for craniofacial reconstruction, Forensic science international, 208 (2011) 95-102.

[40] A. Brunton, A. Salazar, T. Bolkart, S. Wuhrer, Review of statistical shape spaces for 3D data with comparative analysis for human faces, Computer Vision and Image Understanding, 128 (2014) 1-17.

[41] C.W. Hsu, C.C. Chang, C.J. Lin, A practical guide to support vector classification, Tech. Rep., Taipei, 2003.

[42] J. Huang, X. Shao, H. Wechsler, Face pose discrimination using support vector machines (SVM), Proceedings of IEEE on Fourteenth International Conference Pattern Recognition, (1998) 154-156.

[43] C.C. Chang, C.J. Lin, LIBSVM: a library for support vector machines, ACM Transactions on Intelligent Systems and Technology (TIST), 2 (2011) 27.

[44] T.F. Cootes, C.J. Taylor, D.H. Cooper, J. Graham, Active shape models-their training and application, Computer vision and image understanding, 61 (1995) 38-59.

[45] W.D. Turner, R.E. Brown, T.P. Kelliher, P.H. Tu, M.A. Taister, K.W. Miller, A novel method of automated skull registration for forensic facial approximation, Forensic science international, 154 (2005) 149-158.

[46] T.J. Hutton, B.F. Buxton, P. Hammond, Dense surface point distribution models of the human face, IEEE Workshop on Mathematical Methods in Biomedical Image Analysis, (2001) 153-160.

[47] P. Claes, M. Walters, J. Clement, Improved facial outcome assessment using a 3D anthropometric mask, International journal of oral and maxillofacial surgery, 41 (2012) 324-330.

[48] P. Claes, D.K. Liberton, K. Daniels, K.M. Rosana, E.E. Quillen, L.N. Pearson, B. McEvoy, M. Bauchet, A.A. Zaidi, W. Yao, Modeling 3D facial shape from DNA, PLoS Genet, 10 (2014) e1004224.

[49] B. Xia, B. Ben Amor, H. Drira, M. Daoudi, L. Ballihi, Gender and 3D facial symmetry: What's the relationship?, 2013 10th IEEE International Conference and Workshops on Automatic Face and Gesture Recognition (FG), (2013) 1-6.

[50] B. Moghaddam, M.-H. Yang, Learning gender with support faces, IEEE Transactions on Pattern Analysis and Machine Intelligence, 24 (2002) 707-711.

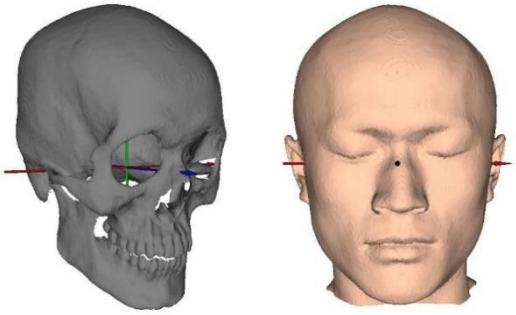

Fig. 1. Skull and corresponding face located in the Frankfurt coordinate system.

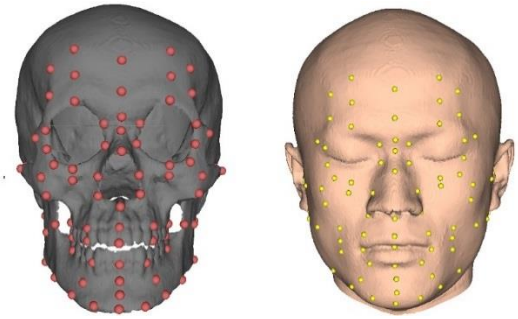

Fig. 2. 78 skull landmarks and the corresponding 78 facial landmarks.

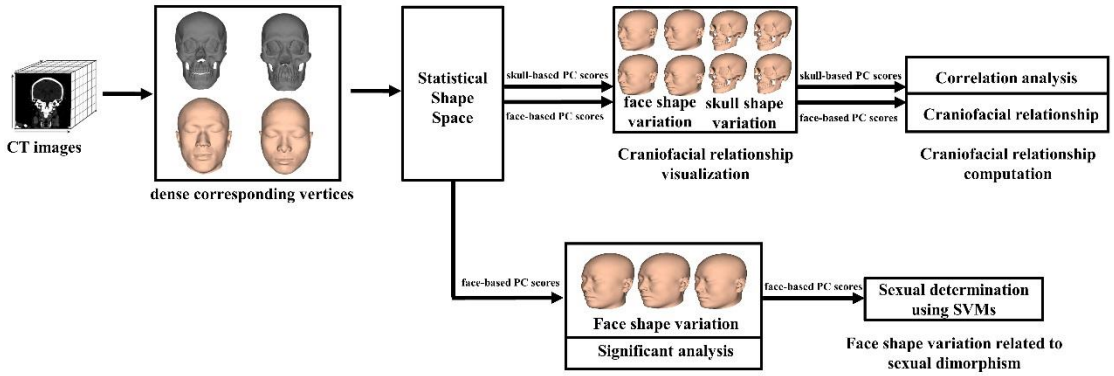

Fig. 3. Overview of the computation of craniofacial relationship and sexual dimorphism of facial shape.

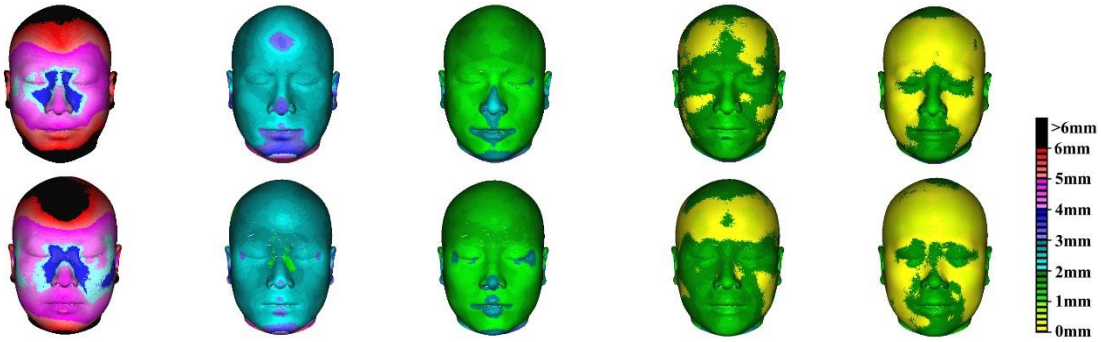

Fig. 4. The quantitative error of every vertex between real face and *PCAface* for male samples (top) and female samples (bottom). From left to right, each figure shows quantitative error using PCs 1, PCs 10, PCs 20, PCs 30 and PCs 35.

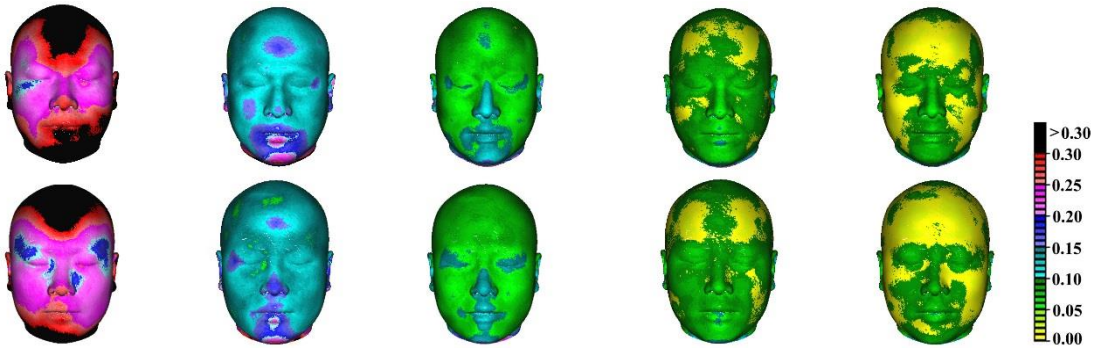

Fig. 5. The standard deviation of every vertex between real face and *PCAface* for male samples (top row) and female samples (bottom row). From left to right, each figure shows standard deviation using PCs 1, PCs 10, PCs 20, PCs 30 and PCs 35.

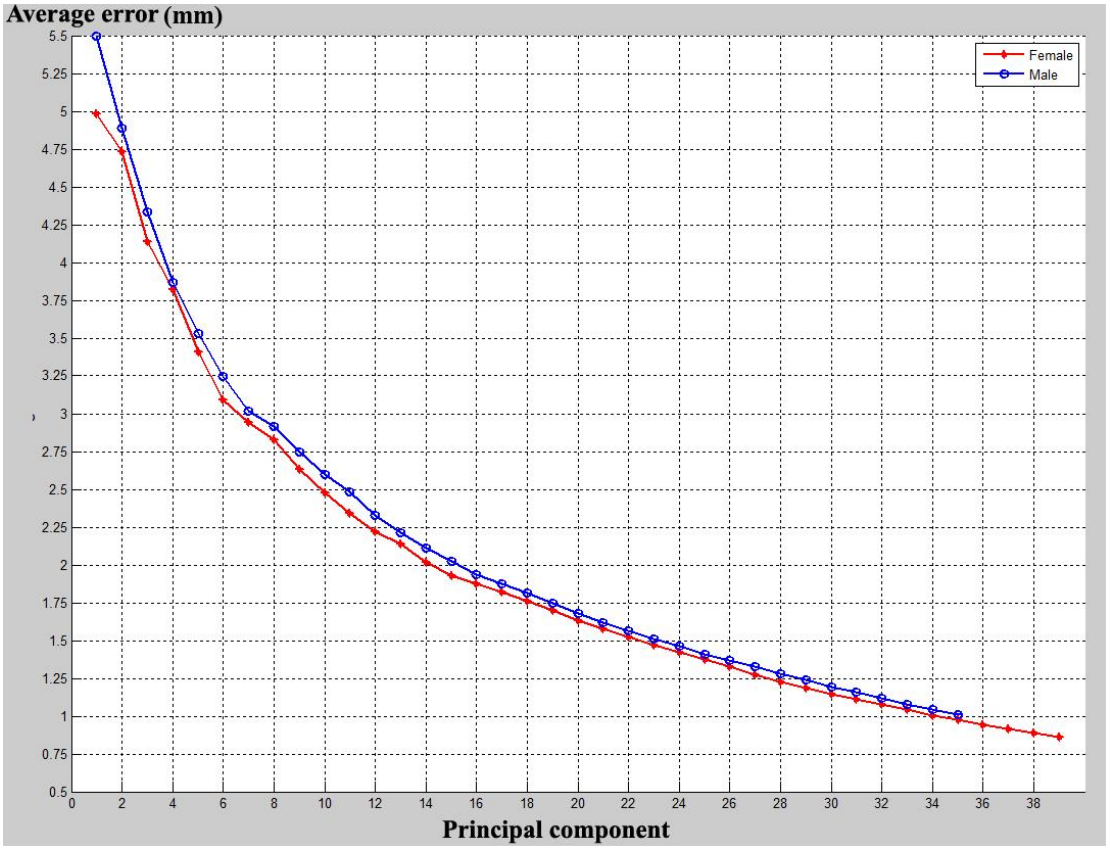

(a)

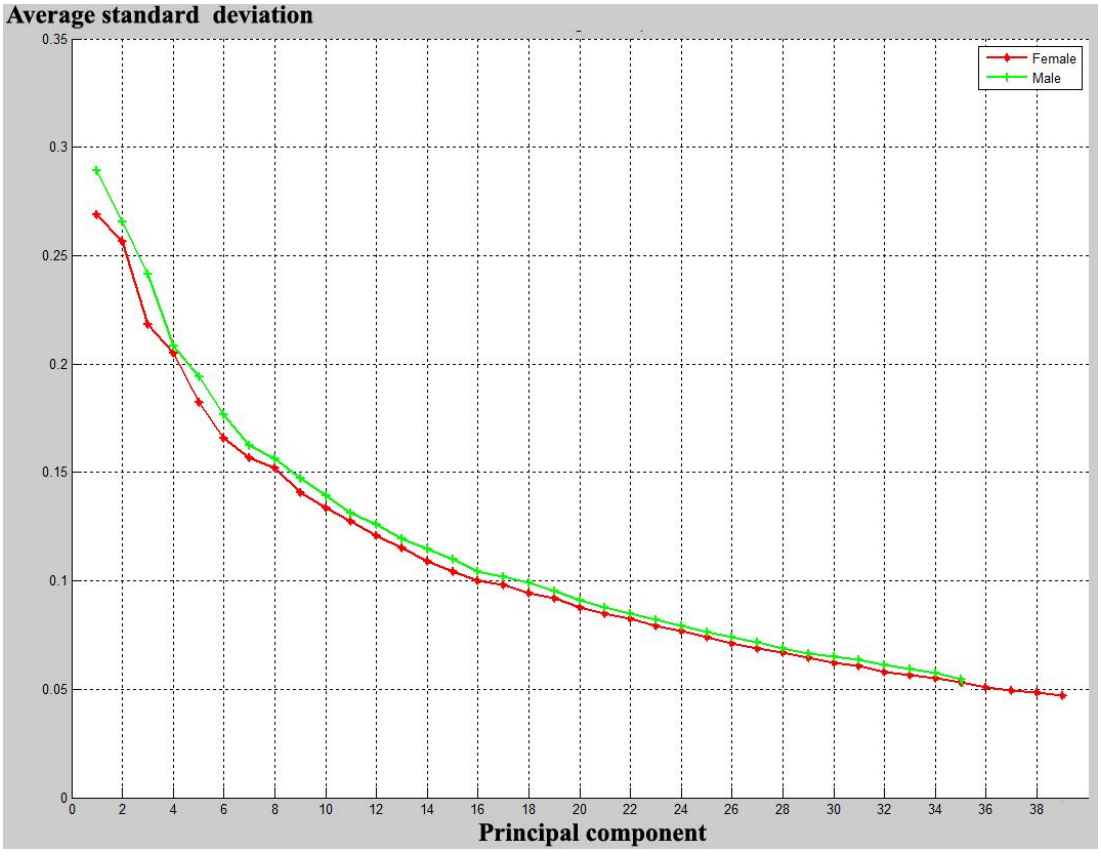

(b)

Fig. 6. The geometric deviations of all the samples between real face and *PCAface* when the number of face-based PCs is increased. (a)

avergError; (b) *avergStd*.

(a)

(b)

Fig. 7. Visualization of skull shape variation captured in PC1, PC2, PC3, PC4 and PC5. From left to right, the weighting coefficient of every PC λ is set to -1.0, -0.6, -0.2, 0.2, 0.6 and 1.0. (a) Front view; (b) Profile view.

(a)

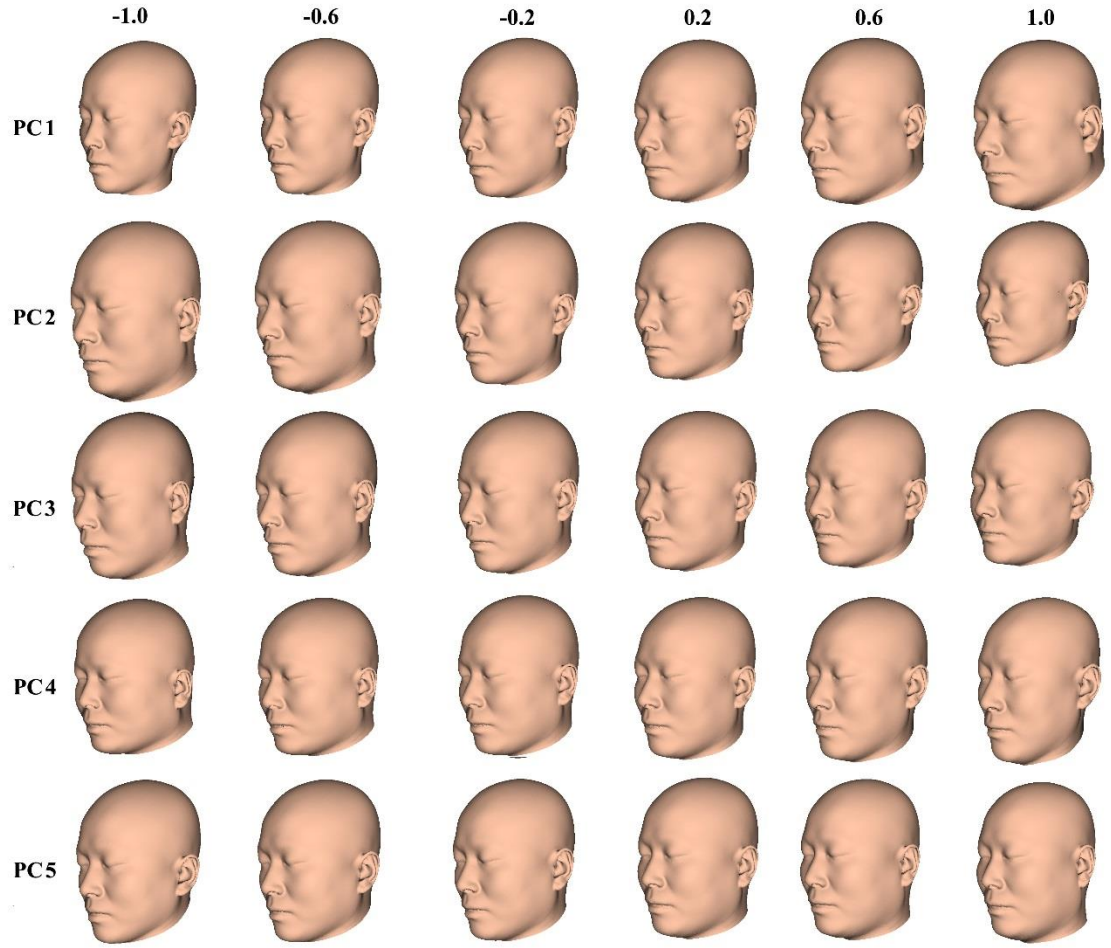

(b)

Fig. 8. Visualization of face shape variation captured in PC1, PC2, PC3, PC4 and PC5. From left to right, the weighting coefficient of every PC λ is set to -1.0, -0.6, -0.2, 0.2, 0.6 and 1.0. (a) Front view; (b) Profile view.

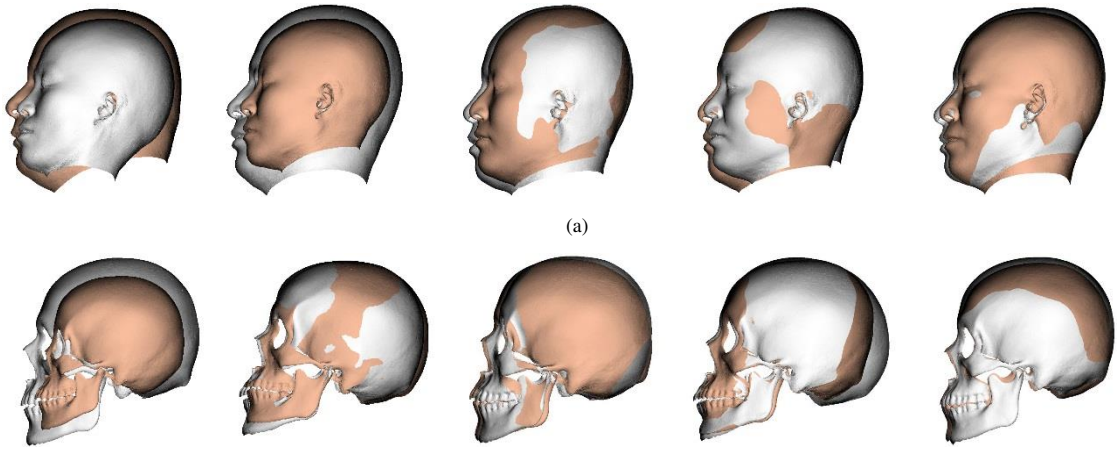

(a)

(b)

Fig. 9. The comparison of shape variation between PCi + (flesh color) and PCi – (grey color). (a) From left to right, each figure shows the influence of PC1, PC2, PC3, PC4 and PC5 on face shape variation. (b) From left to right, each figure shows the influence of PC1, PC2, PC3, PC4 and PC5 on skull shape variation.

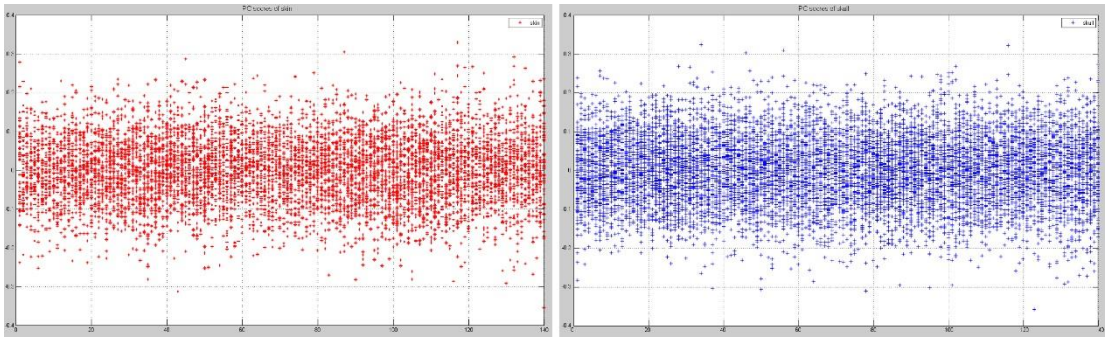

(a)

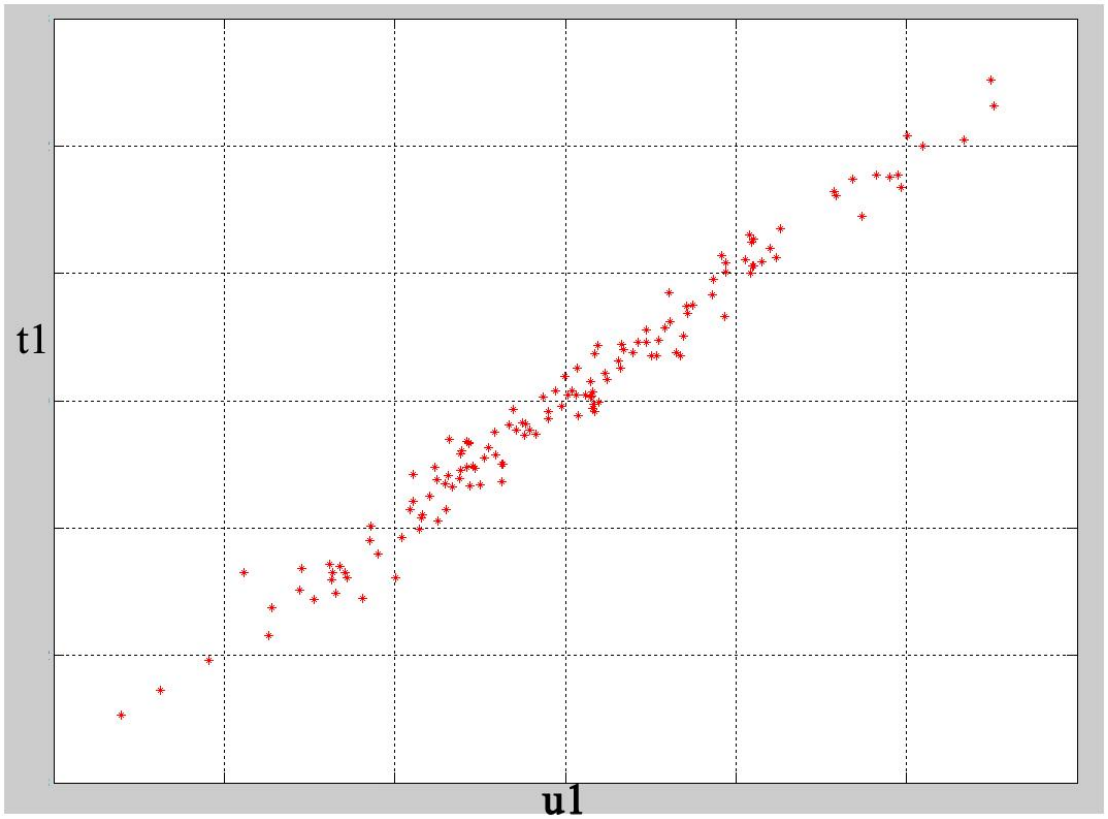

(b)

Fig. 10. Correlation between skull- and face-based PC scores. (a) Face-based (left image) and skull-based (right image) PC scores of every sample within our datasets. (b) The relationships of the first PLS components t1 and u1.

.

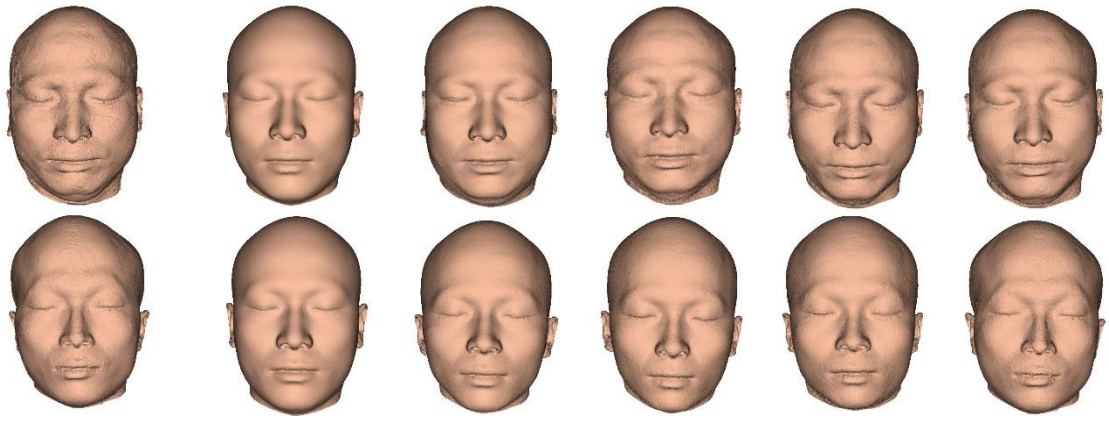

(a)

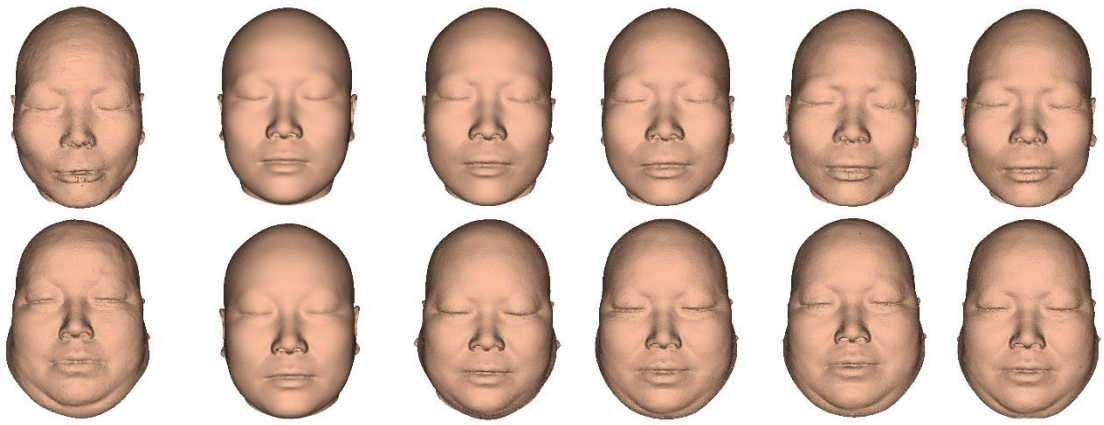

(b)

Fig. 11. Some examples of estimated facial appearances using linear regression. From left to right, each figure shows the real facial appearance and the estimated appearance using PCs 1, PCs 10, PCs 20, PCs 30 and PCs 35. (a) Male examples; (b) Female examples.

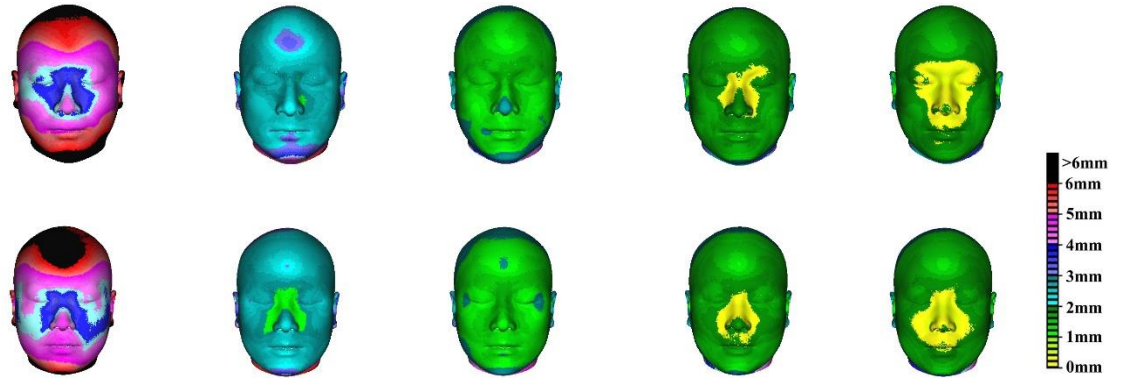

(a)

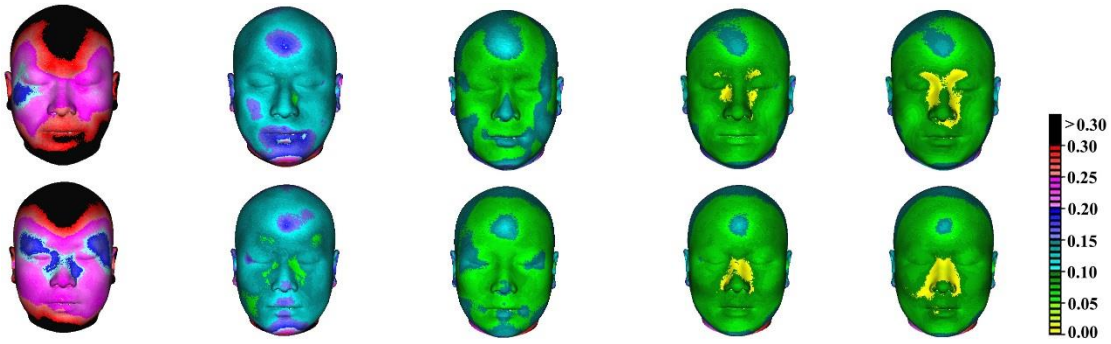

(b)

Fig. 12. The geometric deviations of every vertex between *PCAface* and *estimatedface* for male samples (top row) and female samples (bottom row), when the number of face-based PCs is increased. (a) From left to right, each figure shows quantitative error using PCs 1, PCs 10, PCs 20, PCs 30 and PCs 35. (b) From left to right, each figure shows standard deviation using PCs 1, PCs 10, PCs 20, PCs 30 and PCs 35.

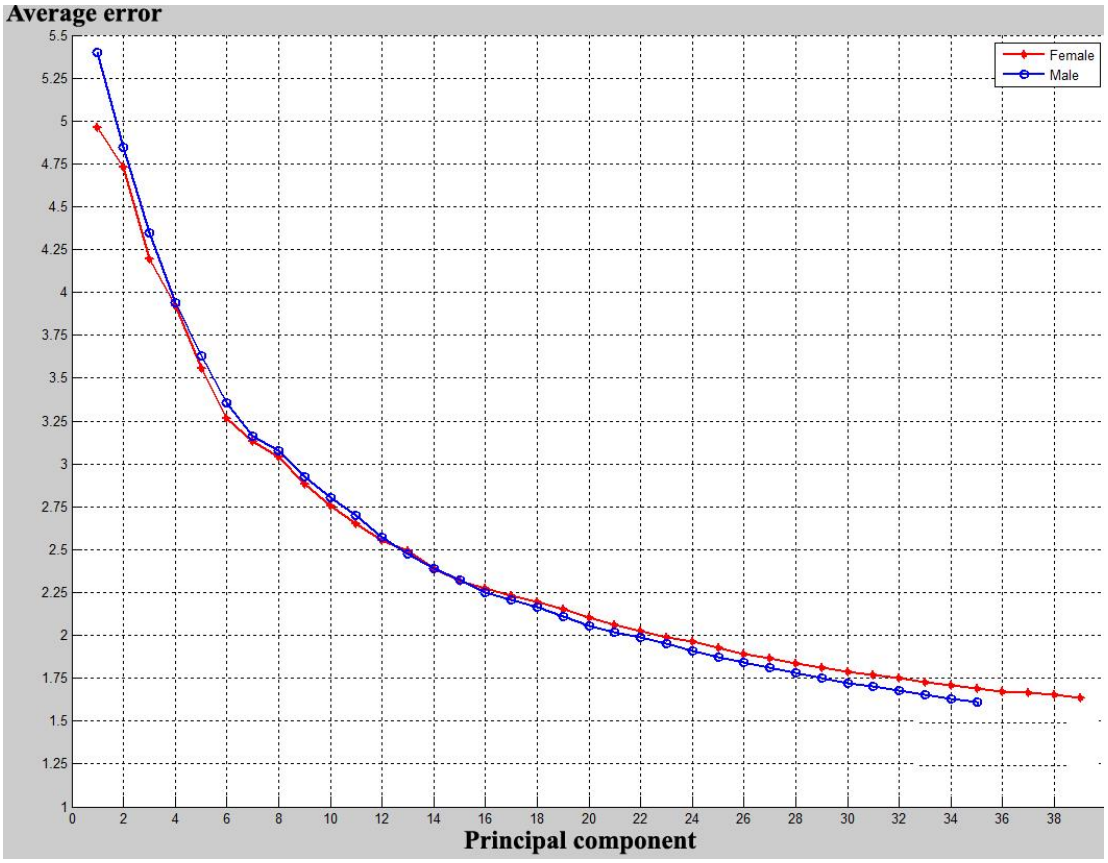
Average error
Female
Male
Principal component

(a)

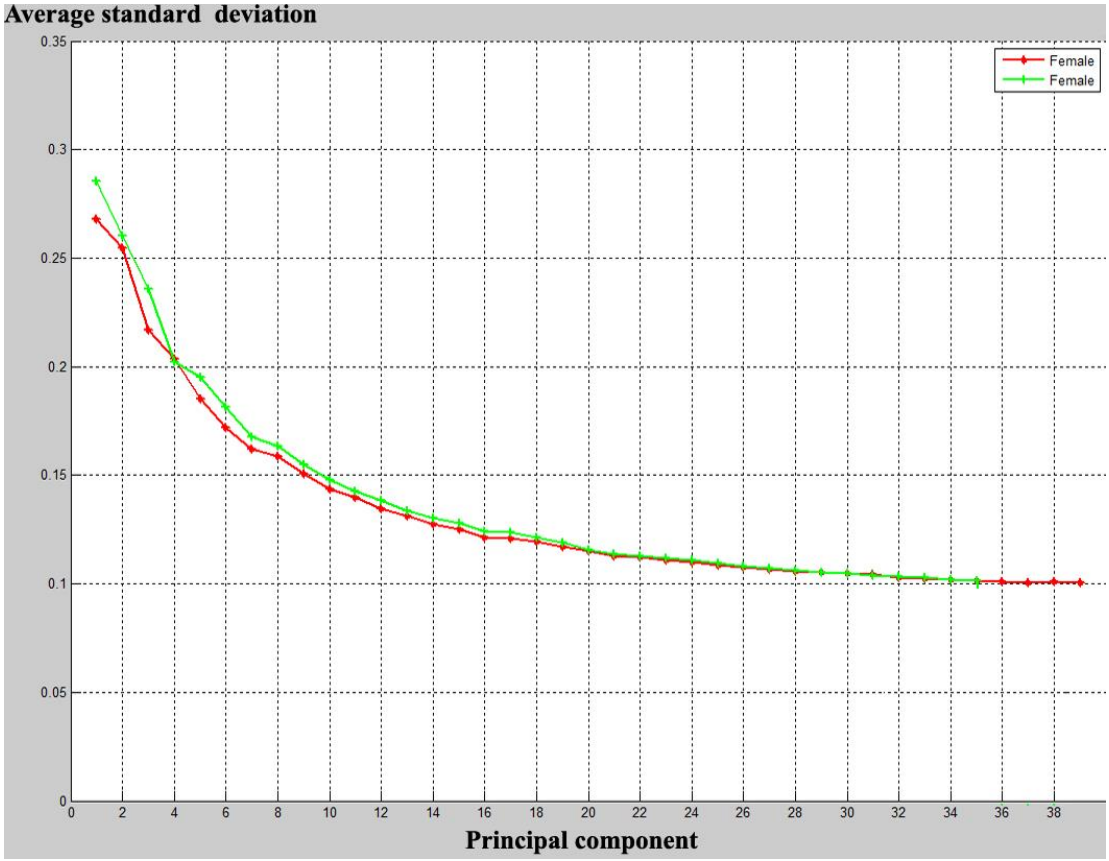
Average standard deviation
Female
Female
Principal component

(b)

Fig. 13. The geometric deviations of all the samples between *PCAface* and *estimatedface* with an increased number of face-based PCs. (a) *avergEstimate*; (b) *avergEstimateStd*.

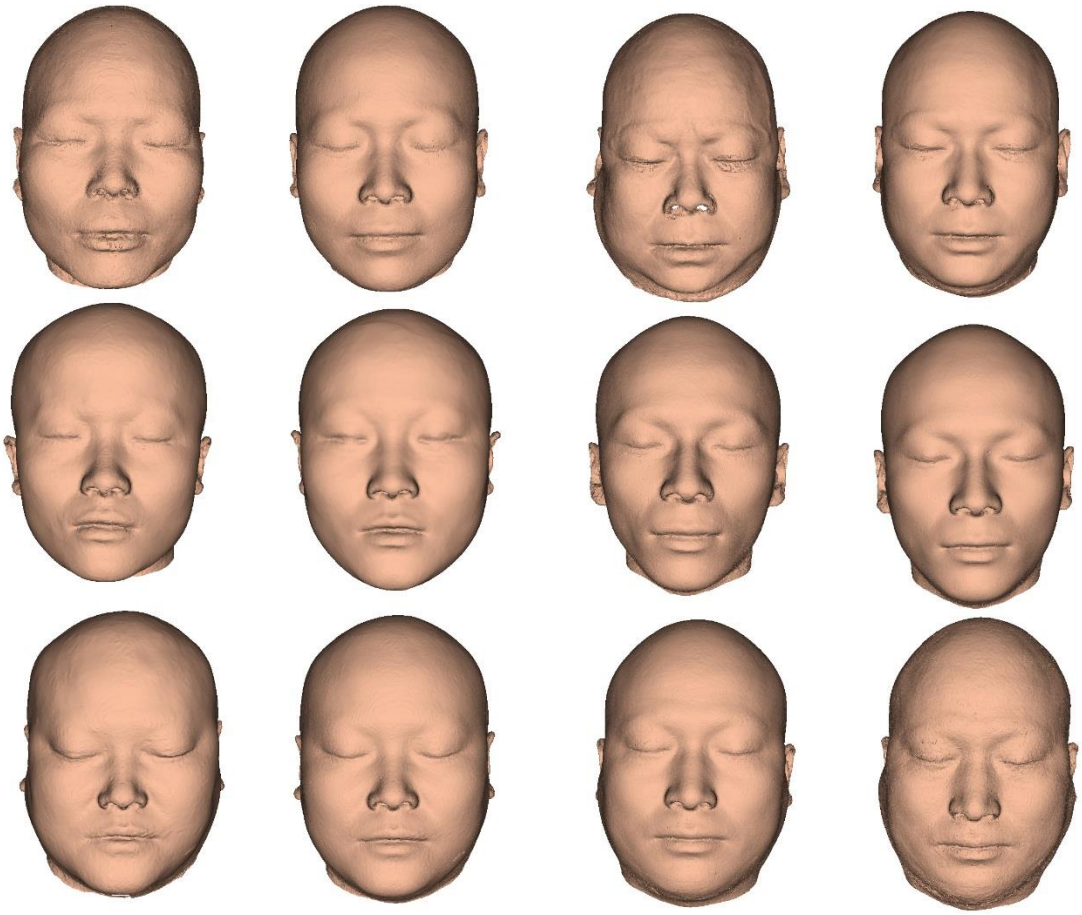

(a) (b)

Fig. 14. Some good examples of estimated facial appearance using the leave-one-out cross validation. Each left figure shows the real facial appearance and the right figure shows the estimated appearance. (a) Female examples; (b) Male examples.

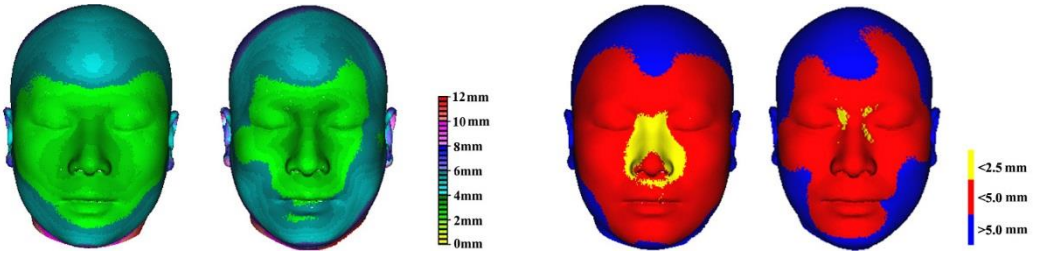

(a)

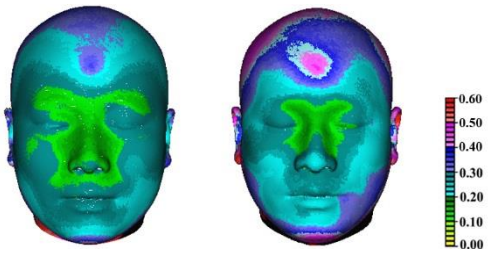

(b)

Fig .15. The geometric deviations of every vertex between *PCAface* and *estimatedface* for female samples (left) and male samples (right) using the leave-one-out method. (a) quantitative error; (b) standard deviation.

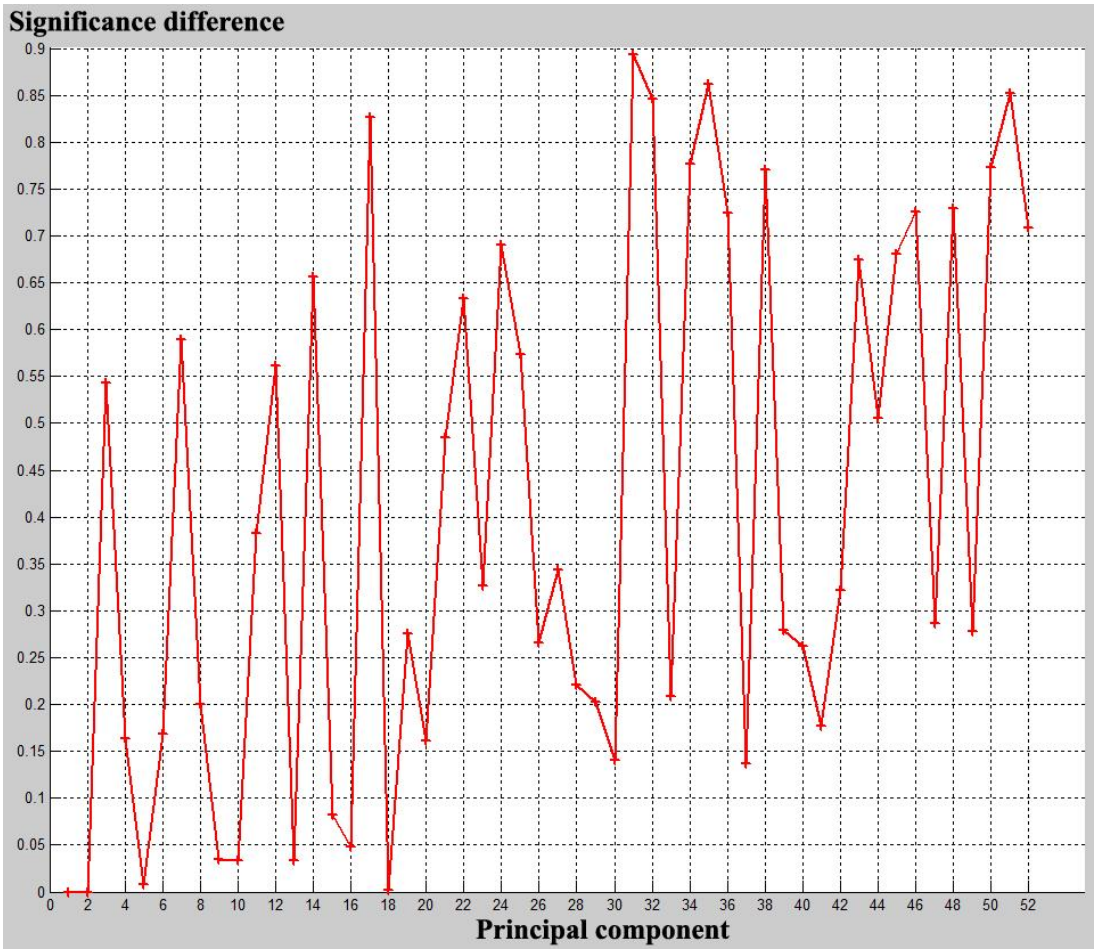
Significance difference
0.9
0.85
0.8
0.75
0.7
0.65
0.6
0.55
0.5
0.45
0.4
0.35
0.3
0.25
0.2
0.15
0.1
0.05
0
0 2 4 6 8 10 12 14 16 18 20 22 24 26 28 30 32 34 36 38 40 42 44 46 48 50 52
Principal component

(a)

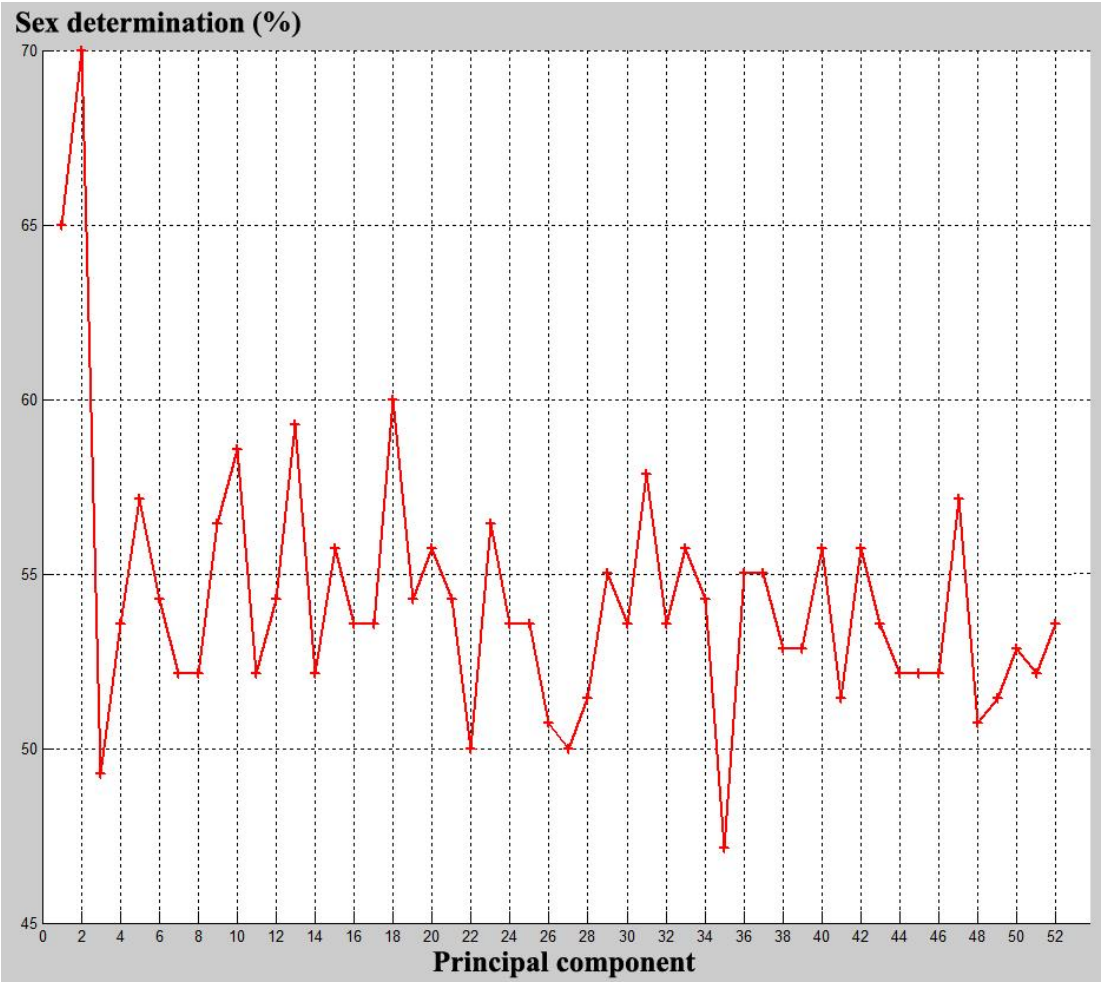

(b)

Fig. 16. The relationship between sex classification and significant difference for every PC. (a) Significant difference analysis; (b) Sex classification rate using SVMs.

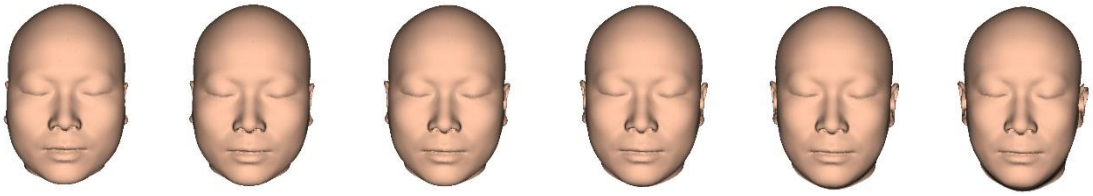

Fig. 17. Face shape variation corresponding to PC18. From left to right, each figure shows the weighting coefficient λ is set to -1.0, -0.6, -0.2, 0.2, 0.6 and 1.0.

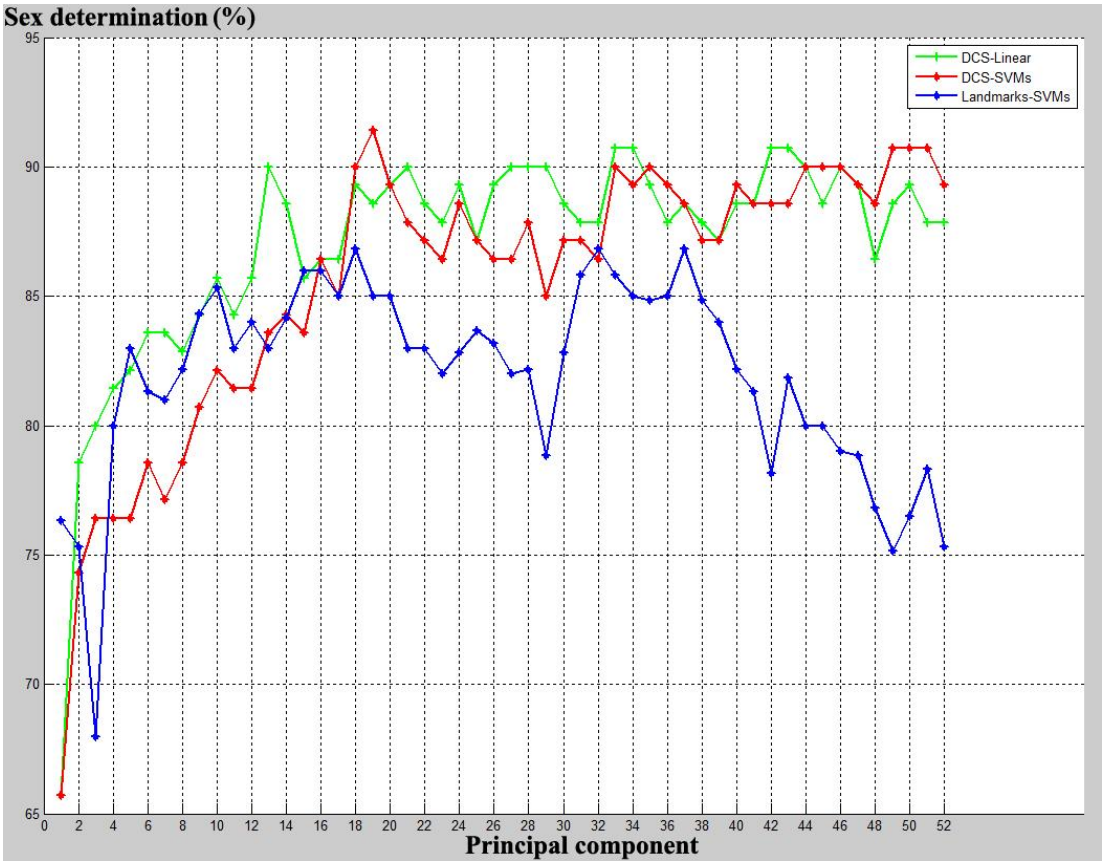

Fig. 18. A comparison of sex classification using three methods.